Dendrochronologia 97 (2026) 126529

Contents lists available at ScienceDirect

Dendrochronologia

journal homepage: www.elsevier.com/locate/dendro

Warming-induced positive age trends challenge MXD detrending

Jan Esper [a,b,*], Ulf Büntgen [b,c,d], Max.C.A. Torbenson [a,e]

[a] Department of Geography, Johannes Gutenberg University, Mainz, Germany
[b] Global Change Research Institute of the Czech Academy of Sciences, Brno, Czech Republic
[c] Department of Geography, University of Cambridge, Cambridge, UK
[d] Department of Geography, Masaryk University, Brno, Czech Republic
[e] Department of Geography, Texas A&M University, College Station, United States

ARTICLE INFO

Keywords:
Maximum latewood density
Tree rings
Standardization
Climate reconstruction
Harz mountains
Germany

ABSTRACT

Raw measurements of maximum latewood density (MXD) typically decline with cambial age. This small but persistent trend may diminish or even reverse in living trees under global warming. We here present such a dataset from the Harz mountains in northern Germany that is characterized by an overall positive age trend retained in 92 MXD series of differently old *Picea abies* trees spanning the period from 1809 to 2020 CE. The positive age trend creates a new situation in which the identification of a temperature signal based on deviations from a horizontal line (e.g. by disabling positive slopes in ARSTAN; Cook, 1985) results in an underestimation of anthropogenic warming, because the residual between the horizontal line and presumed negative age trend remains unconsidered. We approach this problem by testing a range of detrending methods including classic curve fits, signal free (SF), and regional curve standardization (RCS). While none of the methods produces a chronology that perfectly depicts anthropogenic warming, the smallest offset is found when applying RCS to a trimmed MXD dataset. However, the selection of detrending methods based on the fit with instrumental target data, without prior understanding of their suitability, reduces the independency of the proxy record and causes statistical overfitting of the calibration model. Awareness of this problem is important in a rapidly warming world, in which positive age trends in MXD and other temperature-sensitive proxies are likely to increase.

1. MXD measurements and subsets

The Harz MXD dataset is a collection of 92 high-resolution Walesch densitometer profiles from 46 *Picea abies* trees covering the period from 1809 to 2020 CE (Fig. 1). The sampling site is located in 1013 m a.s.l. near the top of the Brocken at 51°47′57″N and 10°36′56″E, a solitary peak in northern Germany likely falling some hundred meters short of a theoretical climatic treeline (Körner and Hoch, 2023). Although the sampled trees range in age from 55 to 220 years, their MXD series are shorter since many trunks are rotten at the inside (see the pith offsets highlighted in grey in Fig. 1**b**).

When aligning all 92 MXD series (hereafter: "All") by cambial age, the mean MXD curve is characterized by a faint but statistically significant positive trend over the first 165 years ($p < 0.05$ for a modified Mann-Kendall test; Hamed and Rao, 1998) followed by an accelerated rise up to an age of 212 years (Fig. 2). This latter acceleration is driven solely by a few very old trees, however. Positive age trends are atypical for MXD datasets, regardless of whether they comprise only living trees covering a few centuries (Briffa et al., 1998; Büntgen et al., 2011; Esper et al., 2010, 2017; Frank and Esper, 2005; Kirdyanov et al., 2024; Torbenson et al., 2025) or combinations of living and dead trees spanning 1000 years and more (Briffa et al., 2013; Büntgen et al., 2006, 2017; Esper et al., 2012, 2014, 2025; Luckman and Wilson, 2005; Schneider et al., 2015).

Unlike many existing MXD chronologies, the new Harz data extends well into the 21st century, so that warming-induced higher MXD values likely triggered the positive age trend in the All collection. This effect becomes visible when aligning only the 30 longest MXD series (hereafter: "Long") that are characterized by a minor negative trend between 50 and 150 years of cambial age (Fig. 2**b**).

The second subset used in this assessment is a trimmed version of the All data produced by removing rings younger than 50 and older than 140 years of cambial age to emulate a composite chronology (hereafter: "Trim"). The resulting 90-year segments are steadily distributed the past 183 years since 1839 CE (green bars in Fig. 1**b**). Trimming not only shortened the mean segment length by almost 100 years compared to

* Corresponding author at: Department of Geography, Johannes Gutenberg University, Mainz, Germany.
E-mail address: esper@uni-mainz.de (Jan Esper).

https://doi.org/10.1016/j.dendro.2026.126529
Received 25 November 2025; Received in revised form 9 April 2026; Accepted 17 April 2026
Available online 17 April 2026

the Long data but also mitigated the chronology age differences ranging from 23 to 195 years in Long to 51–131 years in Trim over the 1839–2020 CE period (Supplementary Fig. S1). Small chronology age differences are a key requirement for successful Regional Curve Standardization (RCS), yet the Trim subset remains far from optimal for this composite detrending method (Esper et al., 2003). This is because the regional curve of the Harz data, i.e. a function of the age-aligned mean curve, is the product of re-aligned tree-rings covering a relatively short period since 1809 CE that is predominantly characterized by warming trends. If the regional curve would be the product of re-aligned tree rings covering the past one or two thousand years, such as in the long composite chronologies cited above, it would represent the site-specific age-related noise independent of prevailing climate trends (Esper et al., 2016; Ljungqvist et al., 2020). Either way, the Trim subset appears more suitable for RCS detrending than All and Long, as it integrates a sequence of relatively short segments distributed over a 183-year period, and the age-aligned mean curve is almost horizontal (Fig. 2**d**).

2. MXD detrending and calibration

We applied six detrending methods (L-Hug, L-Nex, L-SF1, L-SF2, A-RCS, T-RCS) to the Harz MXD data using ratios, arithmetic means, and no variance stabilization. Employing the Harz Long subset, we opted for classic Hugershoff curves including positive slopes (L-Hug) and negative exponential curves excluding positive slopes (L-Nex). Note though that the majority of L-Nex curve fits are substituted by horizontal lines, as ARSTAN (Cook, 1985) uses these as replacements for MXD series with no obvious negative trend (Supplementary Fig. S2). The Long data were also used to run SF detrendings considering the default settings in the RCSsigFree software (Cook et al., 2017) with 50-year age-dependent splines including (L-SF1) and excluding (L-SF2) positive slopes. These runs comprised 12 (L-SF1) and 13 (L-SF2) iterations altering the lower frequency trends of the final chronologies (Supplementary Fig. S3). The two remaining methods were RCS detrendings applied to the All (A-RCS) and Trim (T-RCS) data using 10-year age-dependent splines to approximate the regional curves.

The differently detrended MXD chronologies reveal highly similar calibration stats against regional instrumental data (Rohde et al., 2013) including positive monthly correlations throughout the year of growth,

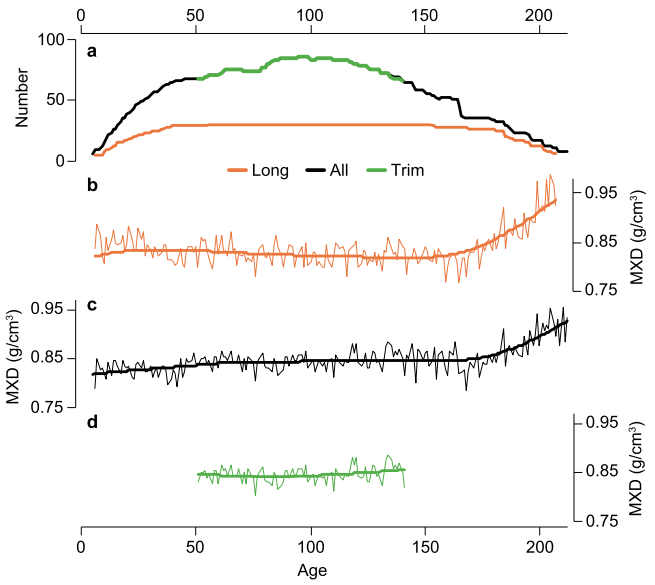

Fig. 2. Age-aligned MXD data. a, Replication curves of the Long (orange), All (black), and Trim (green) Harz MXD data considering pith offsets. b-d, The age-aligned mean MXD curves (thin) and their 100 spline filters (bold).

culminating in the strongest relationship with April-September (A-S) mean temperatures (Fig. 3; Supplementary Fig. S4). L-SF2 returns the highest seasonal correlation over the past 100 years ($r_{1921–2020} = 0.85$), yet the differences among detrendings are statistically insignificant ($p > 0.05$ in a Fisher's z-transformation test; Fisher, 1921). Interestingly, the seasonal correlations become indistinguishable, ranging from $r_{1921–2020} = 0.786–0.789$ across all methods, after first-differencing the MXD and temperature data. This change indicates that *(i)* the larger correlation differences between the original proxy and instrumental data are caused by varying long-term trends, and *(ii)* the changing replication among the All (92 MXD series | 11738 rings), Long (30 | 5242), and Trim (90 | 7056) collections do not affect the inter-annual correlation coefficients. In other words, it was unnecessary to sample and measure more than 30 radii of the old trees to reach the same

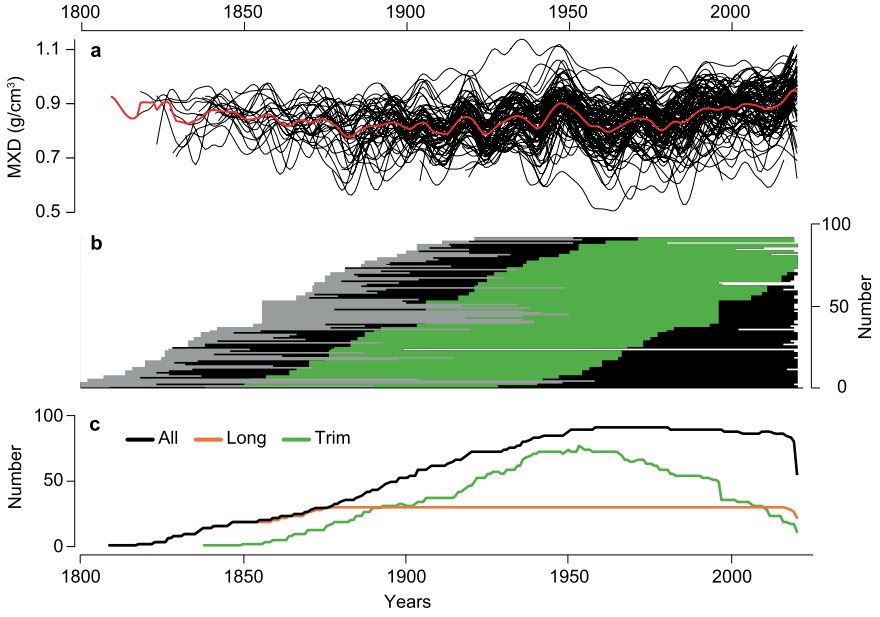

Fig. 1. Harz MXD data. a, 92 MXD series (black) and their mean (red), here smoothed using 10-year splines. b, Bar plot illustrating MXD series lengths. Grey bars indicate pith offsets, black bars tree-rings younger than 90 years and older 140 years, and green bars the rings ranging from 90 to 140 years. c, Replication curves of the full dataset shown in a (black), after trimming the rings < 90 and > 140 years (green), and the 30 longest series (orange).

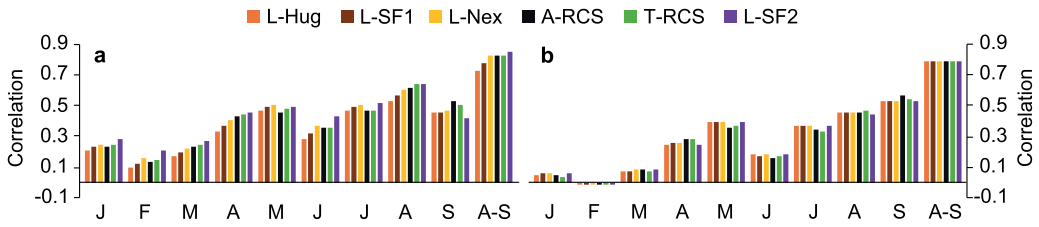

Fig. 3. MXD calibration. a, Monthly and seasonal (April-September) correlations of the differently detrended MXD chronologies (colors) against the nearest Berkeley Earth temperature grid point (Rohde et al., 2013) over the 1921–2020 CE period. b, Same as in a, but after first-differencing the proxy and instrumental data.

high-frequency signal.

3. Temperature divergence

Comparison of the smoothed MXD chronologies with target A-S temperatures reveals substantial trend differences (Fig. 4). Both the classic L-Hug (Briffa et al., 1998) and modern L-SF1 (Melvin and Briffa, 2008) detrendings, permitting positive curve fits, massively underestimate the instrumental warming trend by −1.38°C and −1.14°C in 2020 CE, respectively (Supplementary Fig. S5). This conclusion holds for L-SF1 even though 12 iterative adjustments progressively elevated the post-1980 warming trend in this chronology (Supplementary Fig. S3a).

Temperature divergence is substantially reduced in L-Neg (-0.68°C in 2020 CE) as this method uses linear regressions with zero slope to approximate long-term increasing MXD series. However, restraining detrending curves to a horizontal line still underestimates the targeted warming signal as the residual between the linear regression and presumed negative MXD age trend remains undetected. This limitation does not apply to L-SF2 as the method iteratively adds positive trend to the final chronology (Supplementary Fig. S3b) yet thereby overestimates regional warming by 0.60°C in 2020 CE (maximum in 1996 CE = 0.75°C). This result is achieved using the default settings in the standard RCSsigFree software (Cook et al., 2017). The offset can be mitigated by adjusting program parameters, e.g. by using residuals instead of ratios for detrending (Supplementary Fig. S6). When changing to residuals in RCSsigFree, however, the detrending process is interrupted after six iterations as the convergence tests are not monotonically decreasing, and the resulting chronology shows a reduced modern increase and better fit with target temperatures.

The A-RCS and T-RCS chronologies both underestimate the recorded warming trend (Fig. 4**c**), but the post-1950 CE and 2020 CE residuals are overall smaller, particularly in T-RCS reaching −0.14°C and −0.52°C, respectively (Supplementary Fig. S5b). The reduced divergence in T-RCS is likely driven by the removal of tree-rings < 50 and > 140 years of age and consequential levelling of the chronology age curve (Supplementary Fig. S1) making the Trim subset more suitable for RCS detrending. However, while this finding may appear encouraging in context of the other detrendings employed here, it is important to recall that an offset > 0.5°C in 2020 CE represents more than 1/3 of the maximum warming targeted in 2015 Paris agreement and recorded at hemispheric scale (Esper et al., 2024).

4. Conclusions and outlook

As positive MXD age trends may become more common in a rapidly warming world, classic detrending methods including positive slope fits (e.g. Hugershoff) turn unsuitable (Briffa et al., 1998). The temperature divergence obtained when applying such detrendings is substantially reduced when excluding positive curve fits, yet the methods using horizontal lines as a replacement for positive slope fits inevitably miss a fraction of the warming signal too. This is because the residual between the horizontal line and the presumed (but unknown) negative MXD age

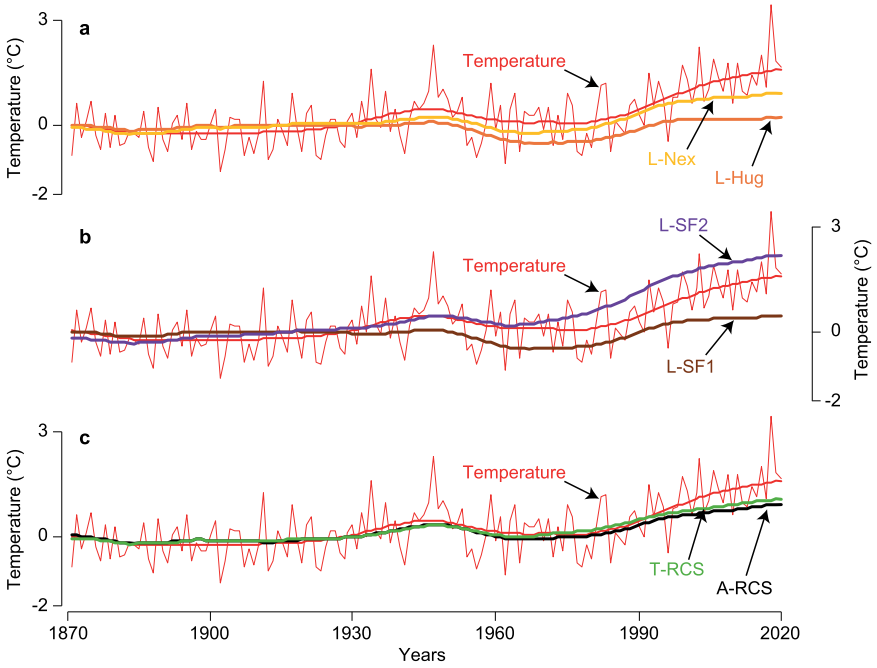

Fig. 4. Temperature fits. a, Original (red) and 30-year smoothed (bold red) April-September temperatures shown together with the smoothed L-Hug (orange) and L-Nex chronologies (yellow) since 1870. b, The same temperatures shown together with the L-SF1 (brown) and L-SF2 (purple) chronologies, and c, together with the A-RCS (black) and T-RCS (green) chronologies. All chronologies were scaled (Esper et al., 2005) from 1870 to 1950 CE to the target temperatures.

trend remains unconsidered.

The state-of-the-art method to identify this missing residual component is SF, in which the measurement series are detrended using expected density curves that are free of the variance shared among trees. However, when this common signal is iteratively reintroduced into the index series, the resulting SF-2 mean chronology overestimates anthropogenic warming by up to 0.75°C. This inverse divergence problem evolved here considering the default settings in RCSsigFree excluding positive slope age-dependent splines. The overestimation can be mitigated using residuals instead of ratios, but the SF run then return warning messages pointing to failing convergence tests. These findings hint to a general problem when applying SF. Whereas the SF theory is accurately detailed (Melvin and Briffa, 2008), the many options and thresholds that can be altered, as well as the subsequently changing iterations, make it impossible to justify ex ante operator decisions. If, however, an ensemble of SF chronologies is produced, e.g. by altering starting spline stiffnesses, convergence test values, convergence tweaks, or else, and the final chronology is selected based on best-fit against instrumental data, this procedure will distort attempts to estimate degrees of freedom of transfer models and uncertainties of derived reconstructions. One could argue to instead add the MXD high frequency variance on the smoothed instrumental temperature trend or even replace the post-1950 MXD chronology with instrumental data, both of which are arguably not very appealing to develop robust climate reconstructions.

The identification of a regionally common age trend is also at the heart of the RCS method, but doing so fundamentally requires tree-ring data distributed over centuries to millennia (Esper et al., 2003). This requirement is frequently violated in tree-ring papers (and also here) where living-tree data are used to establish a regional curve that is supposedly free of the underlying signal. The approach is particularly problematic with temperature-sensitive tree-ring data covering the past 2–4 centuries as the underlying warming trend since the Little Ice Age becomes part of the regional curve and therefore remains undetected when applying RCS. The same problem applies to the Harz MXD data, even though young and old trees have been mixed, so that the resulting A-RCS chronology underestimates modern warming. The problem is not fixed but just mitigated when trimming the data and thereby limiting post-1970 CE tree rings in the regional curve (the green data in Fig. 1**c**). The resulting T-RCS chronology therefore still underestimates warming by > 0.5°C.

We are currently producing more well-replicated MXD chronologies extending into the 2020 s and will explore methods that exclude all post-1970 data affected by accelerated warming to establish signal free regional curves. Until then, it appears important to consider the effects of accelerating warming on tree-ring proxies and potential limitations in preserving robust low frequency variability.

Declaration of Competing Interest

The authors declare that they have no known competing financial interests or personal relationships that could have appeared to influence the work reported in this paper.

Acknowledgements

Supported by the ERC Advanced Grant MONOSTAR (AdG 882727), the ERC Synergy project SYNERGY-PLAGUE (101118880), the co-funded EU project AdAgriF (CZ.02.01.01/00/22_008/0004635), and the German Science Foundation project ES 161/15–1 on wood density methods.

Appendix A. Supporting information

Supplementary data associated with this article can be found in the online version at doi:10.1016/j.dendro.2026.126529.

Data availability

Data will be made available on request.

References

Briffa, K.R., Schweingruber, F.H., Jones, P.D., Osborn, T.J., Shiyatov, S.G., Vaganov, E. A., 1998. Reduced sensitivity of recent tree-growth to temperature at high northern latitudes. Nature 391, 678–682.
Briffa, K.R., Melvin, T.M., Osborn, T.J., Hantemirov, R.M., Kirdyanov, A.V., Mazepa, V. S., Shiyatov, S.G., Esper, J., 2013. Reassessing the evidence for tree-growth and inferred temperature change during the Common Era in Yamalia, northwest Siberia. Quat. Sci. Rev. 72, 83–107.
Büntgen, U., Frank, D.C., Nievergelt, D., Esper, J., 2006. Summer temperature variations in the European Alps, AD 755–2004. J. Clim. 19, 5606–5623.
Büntgen, U., Raible, C.C., Frank, D., Helama, S., Cunningham, L., Hofer, D., Esper, J., 2011. Causes and consequences of past and projected Scandinavian summer temperatures, 500–2100 AD. PLoS One 6, e25133.
Büntgen, U., Krusic, P.J., Verstege, A., Sangüesa-Barreda, G., Wagner, S., Camarero, J.J., Ljungqvist, F.C., Zorita, E., Oppenheimer, C., Konter, O., Tegel, W., Gärtner, H., Cherubini, P., Reinig, F., Esper, J., 2017. New tree-ring evidence from the Pyrenees reveals western Mediterranean climate variability since medieval times. J. Clim. 30, 5295–5318.
Cook, E.R., 1985. A time series analysis approach to tree ring standardization (dendrochronology, forestry, dendroclimatology, autoregressive process). The University of Arizona.
Cook, E.R., Krusic, P.J., Peters, K., Melvin, T., 2017. Program Signal Free (RCSsigFree_Single_MWRE), RCS Signal Free tree–ring standardization program. Tree–Ring Laboratory of Lamont–Doherty Earth Observatory.
Esper, J., Cook, E.R., Krusic, P.J., Peters, K., Schweingruber, F.H., 2003. Tests of the RCS method for preserving low-frequency variability in long tree-ring chronologies. Tree-Ring Res 59, 81–98.
Esper, J., Frank, D.C., Wilson, R.J., Briffa, K.R., 2005. Effect of scaling and regression on reconstructed temperature amplitude for the past millennium. Geophys. Res. Lett. 32, L07711.
Esper, J., Frank, D., Büntgen, U., Verstege, A., Hantemirov, R.M., Kirdyanov, A.V., 2010. Trends and uncertainties in Siberian indicators of 20th century warming. Glob. Change Biol. 16, 386–398.
Esper, J., Frank, D.C., Timonen, M., Zorita, E., Wilson, R.J., Luterbacher, J., Büntgen, U., 2012. Orbital forcing of tree-ring data. Nat. Clim. Change 2, 862–866.
Esper, J., Düthorn, E., Krusic, P.J., Timonen, M., Büntgen, U., 2014. Northern European summer temperature variations over the Common Era from integrated tree-ring density records. J. Quat. Sci. 29, 487–494.
Esper, J., Krusic, P.J., Ljungqvist, F.C., Luterbacher, J., Carrer, M., Cook, E., Büntgen, U., 2016. Ranking of tree-ring based temperature reconstructions of the past millennium. Quat. Sci. Rev. 145, 134–151.
Esper, J., Büntgen, U., Hartl-Meier, C., Oppenheimer, C., Schneider, L., 2017. Northern Hemisphere temperature anomalies during the 1450s period of ambiguous volcanic forcing. Bull. Volcano 79, 41.
Esper, J., Torbenson, M., Büntgen, U., 2024. 2023 summer warmth unparalleled over the past 2000 years. Nature 631, 94–97.
Esper, J., Reinig, F., Torbenson, M., del Castillo, E.M., Kunz, M., Arzac, A., Carrer, M., Chen, F., Kadioglu, A.K., Kirdyanov, A.V., Tejedor, E., Trnka, M., Büntgen, U., 2025. Pan-alpine summer temperatures since 742 CE. Dendrochronologia 94, 126432.
Fisher, R.A., 1921. On the 'probable error' coefficient of correlation deduced from a small sample. Metron 1, 3–32.
Frank, D., Esper, J., 2005. Characterization and climate response patterns of a high-elevation, multi-species tree-ring network in the European Alps. Dendrochronologia 22, 107–121.
Hamed, K.H., Rao, A.R., 1998. A modified Mann-Kendall trend test for autocorrelated data. J. Hydrol. 204, 182–196.
Kirdyanov, A.V., Arzac, A., Kirdyanova, A.A., Arosio, T., Ovchinnikov, D.V., Ganyushkin, D.A., Katjutin, P.N., Myglan, V.S., Nazarov, A.N., Slyusarenko, I.Y., Bebchuk, T., Büntgen, U., 2024. Tree-ring chronologies from the upper treeline in the Russian Altai Mountains reveal strong and stable summer temperature signals. Forests 15, 1402.
Körner, C., Hoch, G., 2023. Not every high-latitude or high-elevation forest edge is a treeline. J. Biogeogr. 50, 838–845.
Ljungqvist, F.C., Piermattei, A., Seim, A., Krusic, P.J., Büntgen, U., He, M., Esper, J., 2020. Ranking of tree-ring based hydroclimate reconstructions of the past millennium. Quat. Sci. Rev. 230, 106074.
Luckman, B.H., Wilson, R.J.S., 2005. Summer temperatures in the Canadian Rockies during the last millennium: a revised record. Clim. Dyn. 24, 131–144.

Melvin, T., Briffa, K.,R., 2008. A "signal-free" approach to dendroclimatic standardisation. Dendrochronologia 26 (2008), 71–86.
Rohde, R., Muller, R.A., Jacobsen, R., Muller, E., Perlmutter, S., Rosenfeld, A., Wickham, C., 2013. A new estimate of the average earth surface land temperature spanning 1753–2011. Geoinf. Geostat. Overv. 1, 1.
Schneider, L., Smerdon, J.E., Büntgen, U., Wilson, R.J., Myglan, V.S., Kirdyanov, A.V., Esper, J., 2015. Revising midlatitude summer temperatures back to AD 600 based on a wood density network. Geophys. Res. Lett. 42, 4556–4562.
Torbenson, M.C.A., Martinez del Castillo, E., Reinig, F., Stahle, D.W., King, K.E., Maxwell, J.T., Harley, G.L., Ziaco, E., Esper, J., 2025. Lack of cold temperatures is driving recent high-summer warming in the southern Rocky Mountains. Int. J. Biometeorol. 69, 1475–1486.